Chapter 2
Pole-Dynamics in Unstable Front Propagation: The Case of The Channel Geometry

Abstract We investigate the problem of flame propagation. This problem is studied as an example of unstable fronts that wrinkle on many scales. The analytic tool of pole expansion in the complex plane is employed to address the interaction of the unstable growth process with random initial conditions and perturbations. We argue that the effect of random noise is immense and that it can never be neglected in sufficiently large systems. We present simulations that lead to scaling laws for the velocity and acceleration of the front as a function of the system size and the level of noise, and analytic arguments that explain these results in terms of the noisy pole dynamics. We makes detailed description of excess number of poles in system, number of poles that appear in the system in unit of time, life time of pole. It allows us to understand dependence of the system parameters on noise.

2.1 Introduction

It must be mentioned that the simplest 1D case of the premixed flame premixed flame front propagation front propagation is very important. It was the main reason for creation this chapter considering in detail the 1D case. Such investigation of this case allows us to understand qualitatively and quantitatively the pole dynamics. This understanding is a basis for the consideration more complex 2D and 3D cases. The papers [26, 30, 85] clearly demonstrate this fact. The cellular structure, acceleration exponent for 2D case was found on the basis of 1D results.

We choose to begin the study with channel geometry. The reason is that in radial geometry it is more difficult to disentangle the effects of external noise from those of initial conditions. After all, initially the system can contain infinitely many poles,very far away near infinity in the complex plane (and therefore having an infinitely small contribution to the interface). Since the growth of the radius changes the stability of the system, more and more of these poles might fall down to the real axis and become observable. In channel geometry the analysis of the effect of initial conditions is relatively straightforward, and one can understand it before focusing on the (more interesting) effects of external noise [48]. The basic reason for this is that in

O. Kupervasser, *Pole Solutions for Flame Front Propagation*,
Mathematical and Analytical Techniques with Applications to Engineering,
DOI 10.1007/978-3-319-18845-4_2

this geometry the noiseless steady state solution for the developed front is known analytically. As described in Sect. 2.2, in a channel of width L the steady-state solution is given in terms of $N(L)$ poles that are organized on a line parallel to the imaginary axis. It can be shown that for any number of poles in the initial conditions this is the only attractor of the pole dynamics. After the establishment of this steady state we can begin to systematically examine the effects of external noise on this solution. As stated before, in radial conditions there is no stable steady state with a finite number of poles, and the disentanglement of initial versus external perturbations is less straightforward ([28] and Chap. 4). We show later that the insights provided in this chapter have relevance for radial growth as well as will be discussed in the sequel.

We have a number of goals in this chapter. Firstly, after introducing the pole decomposition, the pole dynamics, and the basic steady state, we will present stability analysis stability analysis of the solutions of the premixed flame premixed flame propagation problem in a channel geometry. It will be shown that the giant cusp solution is linearly stable, but non-linearly unstable. These results, which are described in Sect. 2.3, can be obtained either by linearizing the dynamics around the giant cusp solutions in order to study the stability eigenvalues, or by examining perturbations in the form of poles in the complex plane. The main result of Sect. 2.3 is that there exists one Goldstone mode and two modes whose eigenvalues hit the real axis periodically when the system size L increases. Thus the system is marginally stable at particular values of L, and it is always nonlinearly unstable, allowing finite size perturbations to introduce new poles into the system. This insight allows us to understand the relation between the system size and the effects of noise. In Sect. 2.4 we discuss the relaxation dynamics that ensues after starting the system with "small" initial data. We study the coarsening process that leads in time to the final solution of the giant cusp, and understand from this what are the typical time scales that exist in our dynamics. We offer in this Section some results of numerical simulations that are interpreted in the later sections. In Sect. 2.5 we focus on the phenomenon of acceleration of the premixed flame front and its relation to the existence of noise. In noiseless conditions the velocity of the premixed flame front in a finite channel is bounded [48]. This can be shown either by using the pole dynamics or directly from the equation of motion. We will present the results of numerical simulations where the noise is controlled, and show how the velocity of the premixed flame front is affected by the level of the noise and the system size. The main results are: (i) Noise is responsible for introducing new poles to the system; (ii) For low levels of noise the velocity of the premixed flame front scales with the system size with a characteristic exponent; (iii) There is a phase transition at a sharp (but system-size dependent) value of the noise-level, after which the behavior of the system changes qualitatively; (iv) After the phase transition the velocity of the premixed flame front changes very rapidly with the noise level. In the last Section we remark on the implications of these observations for the scaling behavior of the radial growth problem, and present a summary and conclusions.

2.2 Equations of Motion and Pole-Decomposition in the Channel Geometry

It is known that planar premixed flames freely propagating through initially motionless homogeneous combustible mixtures are intrinsically unstable. It was reported that such premixed flames develop characteristic structures which include cusps, and that under usual experimental conditions the premixed flame front accelerates as time goes on. A model in $1+1$ dimensions (It is one space and one time dimensions.The space dimensionality of the problem is defined by the space dimensionality of the range of definition for the function, describing moving front) that pertains to the propagation of premixed flame fronts in channels of width $\tilde{L}$ was proposed in [29] (see also Appendix A in this chapter). It is written in terms of position $h(x,t)$ of the premixed flame front above the x-axis. After appropriate rescalings it takes the form:

$$\frac{\partial h(x,t)}{\partial t} = \frac{1}{2}\left[\frac{\partial h(x,t)}{\partial x}\right]^2 + \nu\frac{\partial^2 h(x,t)}{\partial x^2} + I\{h(x,t)\} + 1. \tag{2.1}$$

The domain is $0 < x < \tilde{L}$, ν is a parameter and we use periodic boundary conditions. The functional $I[h(x,t)]$ is the Hilbert transform which is conveniently defined in terms of the spatial Fourier transform

$$h(x,t) = \int_{-\infty}^{\infty} e^{ikx}\hat{h}(k,t)dk \tag{2.2}$$

$$I[h(k,t)] = |k|\hat{h}(k,t) \tag{2.3}$$

For the purpose of introducing the pole-decomposition it is convenient to rescale the domain to $0 < \theta < 2\pi$ (We can to increase the define area of the function $h(\theta,t)$ with periodical boundary condition to $-\infty < \theta < +\infty$ by the periodical continuation). Performing this rescaling and denoting the resulting quantities with the same notation we have

$$\frac{\partial h(\theta,t)}{\partial t} = \frac{1}{2L^2}\left[\frac{\partial h(\theta,t)}{\partial \theta}\right]^2 + \frac{\nu}{L^2}\frac{\partial^2 h(\theta,t)}{\partial \theta^2} + \frac{1}{L}I\{h(\theta,t)\} + 1. \tag{2.4}$$

In this equation $L = \tilde{L}/2\pi$. Next we change variables to $u(\theta,t) \equiv \partial h(\theta,t)/\partial\theta$. We find

$$\frac{\partial u(\theta,t)}{\partial t} = \frac{u(\theta,t)}{L^2}\frac{\partial u(\theta,t)}{\partial \theta} + \frac{\nu}{L^2}\frac{\partial^2 u(\theta,t)}{\partial \theta^2} + \frac{1}{L}I\{u(\theta,t)\}. \tag{2.5}$$

It is well known that the flat front solution of this equation is linearly unstable. The linear spectrum in k-representation is

$$\omega_k = |k|/L - \nu k^2/L^2. \tag{2.6}$$

There exists a typical scale k_{max} which is the last unstable mode

$$k_{max} = \frac{L}{\nu}. \tag{2.7}$$

Nonlinear effects stabilize a new steady-state which is discussed next.

The outstanding feature of the solutions of this equation is the appearance of cusp-like structures in the developing fronts. Therefore a representation in terms of Fourier modes is very inefficient. Rather, it appears very worthwhile to represent such solutions in terms of sums of functions of poles in the complex plane. It will be shown below that the position of the cusp along the front is determined by the real coordinate of the pole, whereas the height of the cusp is in correspondence with the imaginary coordinate. Moreover, it will be seen that the dynamics of the developing front can be usefully described in terms of the dynamics of the poles. Following [28, 47, 48, 50] we expand the solutions $u(\theta, t)$ in functions that depend on N poles whose position $z_j(t) \equiv x_j(t) + iy_j(t)$ in the complex plane is time dependent:

$$\begin{aligned} u(\theta, t) &= \nu \sum_{j=1}^{N} \cot\left[\frac{\theta - z_j(t)}{2}\right] + c.c. \\ &= \nu \sum_{j=1}^{N} \frac{2\sin[\theta - x_j(t)]}{\cosh[y_j(t)] - \cos[\theta - x_j(t)]}, \end{aligned} \tag{2.8}$$

$$h(\theta, t) = 2\nu \sum_{j=1}^{N} \ln\Big[\cosh(y_j(t)) - \cos(\theta - x_j(t))\Big] + C(t). \tag{2.9}$$

In (2.9) $C(t)$ is a function of time; "c.c." means complex conjugate. The function (2.9) is a superposition of quasi-cusps (i.e. cusps that are rounded at the tip). The real part of the pole position (i.e. x_j) is the coordinate (in the domain $[0, 2\pi]$) of the extremum of the quasi-cusp, and the imaginary part of the pole position (i.e. y_j) is related to the depth of the quasi-cusp. As y_j decreases the depth of the cusp increases. As $y_j \to 0$ the depth diverges to infinity. Conversely, when $y_j \to \infty$ the depth decreases to zero.

The main advantage of this representation is that the propagation and wrinkling of the front can be described via the dynamics of the poles. Substituting (2.8) in (2.5) we derive the following ordinary differential equations for the positions of the poles:

$$-L^2\frac{dz_j}{dt} = \left[\nu \sum_{k=1,k\neq j}^{2N} \cot\left(\frac{z_j - z_k}{2}\right) + i\frac{L}{2} sign[Im(z_j)]\right]. \tag{2.10}$$

We note that in (2.8), due to the complex conjugation, we have $2N$ poles which are arranged in pairs such that for $j < N$ $z_{j+N} = \bar{z}_j$. In the second sum in (2.8) each pair of poles contributed one term. In (2.10) we again employ $2N$ poles since all of them interact. We can write the pole dynamics in terms of the real and imaginary parts x_j and y_j. Because of the arrangement in pairs it is sufficient to write the equation for either $y_j > 0$ or for $y_j < 0$. We opt for the first. The equations for the positions of the poles read

$$-L^2\frac{dx_j}{dt} = \nu \sum_{k=1,k\neq j}^{N} \sin(x_j - x_k)\Big[[\cosh(y_j - y_k) \tag{2.11}$$

$$-\cos(x_j - x_k)]^{-1} + [\cosh(y_j + y_k) - \cos(x_j - x_k)]^{-1}\Big]$$

$$L^2\frac{dy_j}{dt} = \nu \sum_{k=1,k\neq j}^{N} \left(\frac{\sinh(y_j - y_k)}{\cosh(y_j - y_k) - \cos(x_j - x_k)}\right.$$

$$\left. + \frac{\sinh(y_j + y_k)}{\cosh(y_j + y_k) - \cos(x_j - x_k)}\right) + \nu\coth(y_j) - L. \tag{2.12}$$

We note that if the initial conditions of the differential equation (2.5) are expandable in a finite number of poles, these equations of motion preserve this number as a function of time. On the other hand, this may be an unstable situation for the partial differential equation, and noise can change the number of poles. This issue will be examined at length in Sect. 2.5.

2.3 Linear Stability Analysis in Channel Geometry

In this section we discuss the linear stability of the TFH-cusp solution. To this aim we first use (2.8) to write the steady solution $u_s(\theta)$ in the form:

$$u_s(\theta) = \nu \sum_{j=1}^{N} \frac{2\sin[\theta - x_s]}{\cosh[y_j] - \cos[\theta - x_s]}, \tag{2.13}$$

where x_s is the real (common) position of the stationary poles and y_j their stationary imaginary position. To study the stability of this solution we need to determine the actual positions y_j. This is done numerically by integrating the equations of motion

for the poles starting from N poles in initial positions and waiting for relaxation. Next one perturbs this solution with a small perturbation $\phi(\theta, t)$: $u(\theta, t) = u_s(\theta) + \phi(\theta, t)$. Linearizing the dynamics for small ϕ results in the equation of motion

$$\frac{\partial \phi(\theta, t)}{\partial t} = \frac{1}{L^2}\Big[\partial_\theta[u_s(\theta)\phi(\theta, t)] + \nu\partial_\theta^2\phi(\theta, t)\Big] + \frac{1}{L}I(\phi(\theta, t)). \tag{2.14}$$

2.3.1 Fourier Decomposition and Eigenvalues

The linear equation can be decomposed in Fourier modes according to

$$\phi(\theta, t) = \sum_{k=-\infty}^{\infty} \hat{\phi}_k(t)e^{ik\theta} \tag{2.15}$$

$$u_s(\theta) = -2\nu i \sum_{k=-\infty}^{\infty}\sum_{j=1}^{N} \text{sign}(k)e^{-|k|y_j}e^{ik\theta} \tag{2.16}$$

In these sums the discrete k values run over all the integers. Substituting in (2.14) we get the equations:

$$\frac{d\hat{\phi}_k(t))}{dt} = \sum_n a_{kn}\hat{\phi}_n(t), \tag{2.17}$$

where a_{kn} is a infinite matrix whose entries are given by

$$a_{kk} = \frac{|\,k\,|}{L} - \frac{\nu}{L^2}k^2 \tag{2.18}$$

$$a_{kn} = \frac{k}{L^2}\text{sign}(k-n)(2\nu\sum_{j=1}^{N} e^{-|k-n|y_j}) \quad k \neq n. \tag{2.19}$$

To solve for the eigenvalues of this matrix we need to truncate it at some cutoff k-vector k^*. The choice of k^* can be based on the linear stability analysis of the flat front. The scale k_{max}, cf. (2.7), is the largest k which is still linearly unstable. We must choose $k^* > k_{max}$ and test the choice by the converegence of the eigenvalues. The chosen value of k^* in our numerics was $4k_{max}$. The results for the low order eigenvalues of the matrix a_{kn} that were obtained from a converged numerical calculation are presented in Fig. 2.1.

The eigenvalues are multiplied by L^2 and are plotted as a function of L. We order the eigenvalues in decreasing order and denote them as $|\,\lambda_0\,| \leq |\,\lambda_1\,| \leq |\,\lambda_2\,| \cdots$

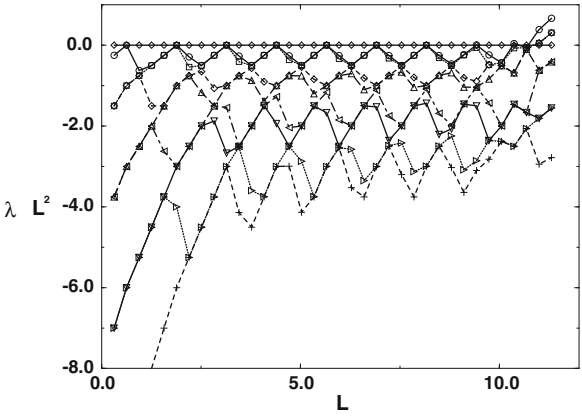

Fig. 2.1 The first 10 highest eigenvalues of the stability matrix with $\nu = \pi/5$, multiplied by the *square* of the system size L^2 versus the system size L. Note that all the eigennvalues oscillate around fixed values in this presentation, and that the highest two eigenvalues hit zero periodically

Figure 2.1 contains a strange result on the positive eigenvalues at large L. One of methods to check some numerical result is to do analytic investigation. For example, in Chap. 3 we make detailed analytic investigation for the numerical result on Fig. 2.1 and obtain that all eigenvalues are not positive. Indeed, two types of modes exists. The first one is connected to the displacement of poles in the giant cusp. Because of the pole attraction the giant cusp is stable with respect to the longitudinal displacement of poles and so the correspondent eigenvalues are not positive. For the transversal displacement the Lyapunov function exists and so the giant cusp is stable with respect to the transversal displacement and the correspondent eigenvalues are not positive. The second type of modes is connected to additional poles. These poles go to infinity because of the repulsion from the giant cusp poles $N(L)$. So the correspondent eigenvalues are also not positive. So the positive eigenvalues at large L are a result of numerical errors.

The figure offers a number of qualitative observations:

1. There exists an obvious Goldstone or translational mode $u_s'(\theta)$ with eigenvalue $\lambda_0 = 0$, which is shown with rhombes in Fig. 2.1. This eigenmode stems from the Galilean invariance of the equation of motion.
2. The eigenvalues oscillate periodically between values that are L-independent in this presentation (in which we multiply by L^2). In other words, up to the oscillatory behavior the eigenvalues depend on L like L^{-2}.
3. The eigenvalues λ_1 and λ_2, which are represented by squares and circles in Fig. 2.1, hit zero periodically. The functional dependence in this presentation appears almost piecewise linear.
4. The higher eigenvalues also exhibit similar qualitative behaviour, but without reaching zero. We note that the solution becomes marginally stable for every value of L for which the eigenvalues λ_1 and λ_2 hit zero. The L^{-2} dependence of the spectrum indicates that the solution becomes more and more sensitive to noise as L increases.

2.3.2 Qualitative Understanding Using Pole-Analysis

The most interesting qualitative aspects are those enumerated above as item 2 and 3. To understand them it is useful to return to the pole description, and to focus on (2.11). This equation describes the dynamics of a single far-away pole. We remarked before that this equation shows that for *fixed* L the stable number of poles is the integer part Eq. (1.10). Define now the number α, $0 \leq \alpha \leq 1$, according to

$$\alpha = \left[\frac{1}{2}\left(\frac{L}{\nu}+1\right)\right] - \frac{1}{2}\left(\frac{L}{\nu}-1\right). \tag{2.20}$$

Using this number we rewrite (2.11) as

$$\frac{dy_a}{dt} \approx \frac{2\nu}{L^2}\alpha. \tag{2.21}$$

As L increases, α oscillates piecewise linearly and periodically between zero and unity. This shows that a distant pole which is added to the giant cusp solution is usually repelled to infinity except when α hits zero and the system becomes marginally unstable to the addition of a new pole.

To connect this to the linear stability analysis we note from (2.8) that a single far-away pole solution (i.e. with y very large) can be written as

$$u(\theta, t) = 4\nu e^{-y(t)} \sin(\theta - x(t)). \tag{2.22}$$

Suppose that we add to our giant cusp solution a perturbation of this functional form. From (2.21) we know that y grows linearly in time, and therefore this solution decays exponentially in time. The rate of decay is a linear eigenvalue of the stability problem, and from (2.21) we understand both the $1/L^2$ dependence and the periodic marginality. We should note that this way of thinking gives us a significant part of the L dependence of the eigenvalues, but not all. The variable α is rising from zero to unity periodically, but after reaching unity it hits zero instantly. Accordingly, if the highest non zero eigenvalue were fully determined by the pole analysis, we would expect this eigenvalue to behave as the solid line shown in Fig. 2.2.

The actual highest eigenvalue computed from the stability matrix is shown in rhombuses connected by dotted line. It is clear that the pole analysis gives us a great deal of qualitative and quantitative understanding, but not all the features agree.

2.3.3 Dynamics Near Marginality

The discovery of marginality at isolated values of L poses questions regarding the fate of poles that are added at very large y's at certain x-positions. We will argue now that when the system becomes marginally stable, a new pole can be added to those

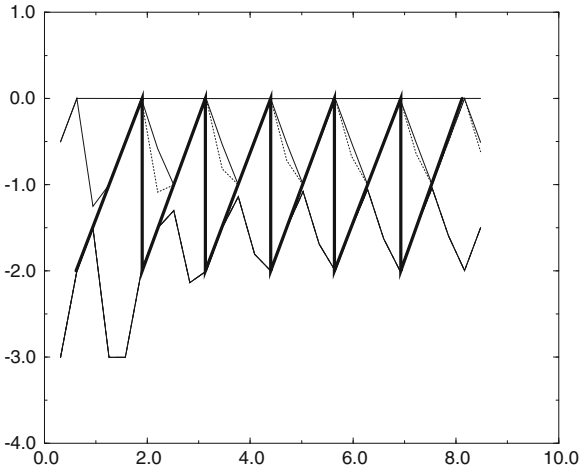

Fig. 2.2 Comparison of the numerically determined highest 4 eigenvalues of the stability matrix with the prediction of the pole analysis. The eigenvalues of the stability matrix are: λ_0, λ_1, λ_2 and λ_3. The pole analysis (*solid line*) provides a qualitative understanding of the stability, and appears to overlap with the high est eigenvector over half of the range, and with the fourth eigenvalue over the other half

existing in the giant cusp. We remember that these poles have a common θ position that we denote as $\theta = \theta_c$. The fate of a new pole added at infinity depends on its θ position. If the position of the new pole is again denoted as y_a, and $\infty \gg y_a \gg y_{max}$, we can see from (2.12) that dy_a/dt is maximal when $\theta_a = \theta_c$, whereas it is minimal when $\theta_a - \theta_c = \pi$. This follows from the fact that the cosine term has a value $+1$ when $\theta_a = \theta_c$ and a value -1 when $\theta_a - \theta_c = \pi$. For large y differences the terms in the sum take on their minimal value when the cos term is -1 and their maximal values at $+1$. For infinitely large y_a the equation of motion is (11) which is independent of θ_a. Since the RHS of this equation becomes zero at marginality, we conclude that for very large but finite y_a dy_a/dt changes sign from positive to negative when $\theta_a - \theta_c$ changes from zero to π. The meaning of this observation is that the most unstable points in the system are those points which are furthest away from the giant cusp. It is interesting to discuss the fate of a pole that is added to the system at such a position. From the point of view of the pole dynamics $\theta = \theta_c + \pi$ is an unstable fixed point for the motion along the θ axis. The attraction to the giant cusp exactly vanishes at this point. If we start with a pole at a very large y_a close to this value of θ the down-fall along the y coordinate will be faster than the lateral motion towards the giant cusp. We expect to see therefore the creation of a small cusp at θ values close to π that precedes a later stage of motion in which the small cusp moves to merge with the giant cusp. Upon the approach of the new pole to the giant cusp all the existing poles will move up and the furthest pole at y_{max} will be kicked off to infinity. We will later explain that this type of dynamics occurs in stable systems that are driven by noise. The noise generates far away poles (in the imaginary direction) that get attracted around $\theta = \theta_c + \pi$ to create small cusps that run continuously towards the giant cusp.

2.3.4 Excitable System

The intuition gained so far can be used to discuss the issue of stability of a stable system to *larger* perturbations. In other words, we may want to add to the system poles at finite values of y and ask about their fate. We first show in this subsection that poles whose initial y value is below $y_{max} \sim \log(L^2/\nu^2)$ will be attracted towards the real axis. The scenario is similar to the one described in the last paragraph.

Suppose that we generate a stable system with a giant cusp at $\theta_c = 0$ with poles distributed along the y axis up to y_{max}. We know that the sum of all the forces that act on the upper pole is zero. Consider then an additional pole inserted in the position (π, y_{max}). It is obvious from (2.12) that the forces acting on this pole will pull it downward. On the other hand if its initial position is much above y_{max} the force on it will be repulsive towards infinity. We see that this simple argument identifies y_{max} as the typical scale for nonlinear instability.

Next we estimate y_{max} and interpret our result in terms of the *amplitude* of a perturbation of the premixed flame front. We explained that uppermost pole's position fluctuates between a minimal value and infinity as L is changing. We want to estimate the characteristic scale of the minimal value of $y_{max}(L)$. To this aim we employ the result of [48] regarding the stable distribution of pole positions in a stable large system. The parametrization of [48] differs from ours; to go from our parametrization in (2.5) to theirs we need to rescale u by L^{-1} and t by L. The parameter ν in their parameterizations is ν/L in ours. According to [48] the number of poles between y and $y + dy$ is given by the $\rho(y)dy$ where the density $\rho(y)$ is

$$\rho(y) = \frac{L}{\pi^2 \nu} \ln[\coth(|y|/4)]. \tag{2.23}$$

To estimate the minimal value of y_{max} we require that the tail of the distribution $\rho(y)$ integrated between this value and infinity will allow one single pole. In other words,

$$\int_{y_{max}}^{\infty} dy \rho(y) \approx 1. \tag{2.24}$$

Expanding (2.23) for large y and integrating explicitly the result in (2.24) we end up with the estimate

$$y_{max} \approx 2 \ln \left[\frac{4L}{\pi^2 \nu} \right] \tag{2.25}$$

For large L this result is $y_{max} \approx \ln(\frac{L^2}{\nu^2})$. If we now add an additional pole in the position (θ, y_{max}) this is equivalent to perturbing the solution $u(\theta, t)$ with a function $\nu e^{-y_{max}} \sin(\theta)$, as can be seen directly from (2.8). We thus conclude that the system is unstable to a perturbation *larger* than

$$u(\theta) \sim \nu^3 \sin(\theta)/L^2. \tag{2.26}$$

This indicates a very strong size dependence of the sensitivity of the giant cusp solution to external perturbations. This will be an important ingredient in our discussion of noisy systems.

2.4 Initial Conditions, Pole Decomposition and Coarsening

In this section we show first that any initial conditions can be approximated by pole decomposition. Later, we show that the dynamics of sufficiently smooth initial data can be well understood from the pole decomposition. Finally we employ this picture to describe the *inverse cascade* of cusp into the giant cusp which is the final steady state. By inverse cascade we mean a nonlinear coarsening process in which the small scales coalesce in favor of larger scales and finally the system saturates at the largest available scale [91].

2.4.1 Pole Expansion: General Comments

The fundamental question is how many poles are needed to describe any given initial condition. The answer, of course, depends on how smooth are the initial conditions. Suppose also that we have an initial function $u(\theta, t = 0)$ that is 2π-periodic and which at time $t = 0$ admits a Fourier representation

$$u(\theta) = \sum_{k=1}^{\infty} A_k \sin(k\theta + \phi_k), \tag{2.27}$$

with $A_k > 0$ for all k. Suppose that we want to find a pole-decomposition representation $u_p(\theta)$ such that

$$|u_p(\theta) - u(\theta)| \leq \epsilon \qquad \text{for every } \theta, \tag{2.28}$$

where ϵ is a given wanted accuracy. If $u(\theta)$ is differentiable we can cut the Fourier expansion at some finite $k = K$ knowing that the remainder is smaller than, say, $\epsilon/2$. Choose now a large number M and a small number $\Delta \ll 1/M$ and write the pole representation for $u_p(\theta)$ as

$$u_p(\theta) = \sum_{k=1}^{K} \sum_{p=0}^{M-1} \frac{2k \sin(k\theta + \phi_k)}{\cosh[k(y_k + p\Delta)] - cos(k\theta + \phi_k)}. \tag{2.29}$$

To see that this representation is a particular form of the general formula (2.8) We use the following two identities

$$\sum_{k=0}^{\infty} e^{-kt} \sin xk = \frac{1}{2} \frac{\sin x}{\cosh t - \cos x}, \tag{2.30}$$

$$\sum_{k=0}^{K-1} \sin(x + ky) = \sin\left(x + \frac{K-1}{2} y\right) \sin \frac{Ky}{2} \operatorname{cosec} \frac{y}{2}. \tag{2.31}$$

From these follows a third identity

$$\sum_{j=0}^{K-1} \frac{2 \sin\left(x - \frac{2\pi j}{K} + \phi\right)}{\cosh y - \cos\left(x - \frac{2\pi j}{K} + \phi\right)} = \frac{2K \sin(Kx + \phi)}{\cosh Ky - \cos(Kx + \phi)}. \tag{2.32}$$

Note that the LHS of (2.32) is of the form (2.8) with K poles whose positions are all on the line $y_j = y$ and whose x_j are on the lattice points $2\pi j/K - \phi$. On the other hand every term in (2.29) is of this form.

Next we use (2.30) to rewrite (2.29) in the form

$$u_p(\theta) = \sum_{k=1}^{K} \sum_{p=0}^{M-1} \sum_{n=1}^{\infty} 4k e^{-nk(y_k + p\Delta)} \sin(nk\theta + n\phi_k). \tag{2.33}$$

Exchanging order of summation between n and p we can perform the geometric sum on p. Denoting

$$b_{n,k} \equiv \sum_{p=0}^{M-1} e^{-nkp\Delta} = \frac{1 - e^{-Mkn\Delta}}{1 - e^{-kn\Delta}}, \tag{2.34}$$

we find

$$\begin{aligned} u_p(\theta) &= \sum_{k=1}^{K} \sum_{n=1}^{\infty} 4k b_{n,k} e^{-nky_k} \sin(nk\theta + n\phi_k) \\ &= \sum_{k=1}^{K} \sum_{n=2}^{\infty} 4k b_{n,k} e^{-nky_k} \sin(nk\theta + n\phi_k) \\ &\quad + \sum_{k=1}^{K} 4k b_{1,k} e^{-ky_k} \sin(k\theta + \phi_k). \end{aligned} \tag{2.35}$$

Compare now the second term on the RHS of (2.35) with (2.27). We can identify

$$e^{-ky_k} = \frac{A_k}{4kb_{1,k}} \tag{2.36}$$

The first term can be then bound from above as

$$\begin{aligned} &\Big| \sum_{k=1}^{K} \sum_{n=2}^{\infty} 4kb_{n,k} e^{-nky_k} \sin\left(nk\theta + n\phi_k\right) \Big| \\ &\leq \sum_{k=1}^{K} \sum_{n=2}^{\infty} \Big| 4kb_{n,k} \left[\frac{A_k}{4kb_{1,k}} \right]^n \sin\left(nk\theta + n\phi_k\right) \Big|. \end{aligned} \tag{2.37}$$

The sine function and the factor $(4K)^{1-n}$ can be replaced by unity and we can bound the RHS of (2.37) by

$$\sum_{k=1}^{K} \sum_{n=2}^{\infty} \left[\frac{A_k}{b_{1,k}} \right]^n b_{n,k} \leq \sum_{k=1}^{K} A_k \sum_{n=1}^{\infty} \left[\frac{A_k}{b_{1,k}} \right]^n, \tag{2.38}$$

where we have used the fact that $b_{n,k} \leq b_{1,k}$ which follows directly from (2.34). Using now the facts that $b_{1,K} \leq b_{1,k}$ for every $k \leq K$ and that A_k is bounded by some finite C since it is a Fourier coefficient, we can bound (2.38) by $C^2K/(b_{1,K} - C)$. Since we can select the free parameters Δ and M to make $b_{1,K}$ as large as we want, we can make the remainder series smaller in absolute value than $\epsilon/2$.

The conclusion of this demonstration is that any initial condition that can be represented in Fourier series can be approximated to a desired accuracy by pole-decomposition. The number of needed poles is of the order $K^2 \times M$. Of course, the number of poles thus generated by the initial conditions may exceed the number $N(L)$ found in (2.10). In such a case the excess poles will move to infinity and will become irrelevant for the short time dynamics. Thus a smaller number of poles may be needed to describe the state at larger times than at $t = 0$. We need to stress at this point that the pole decomposition is over complete; for example, if there is exactly one pole at $t = 0$ and we use the above technique to reach a pole decomposition we would get a large number of poles in our representation.

2.4.2 *The Initial Stages of the Front Evolution: The Exponential Stage and the Inverse Cascade*

In this section we employ the connection between Fourier expansion and pole decomposition to understand the initial exponential stage of the evolution of the premixed flame front with small initial data $u(\theta, t = 0)$. Next we employ our knowledge of the pole interactions to explain the slow dynamics of coarsening into the steady state solution.

Suppose that initially the expansion (2.27) is available with all the coefficients $A_k \ll 1$. We know from the linear instability of the flat premixed flame front that each Fourier component changes exponentially in time according to the linear spectrum (2.6). The components with wave vector larger than (2.7) decrease, whereas those with lower wave vectors increase. The fastest growing mode is $k_c = L/2\nu$. In the linear stage of growth this mode will dominate the shape of the premixed flame front, i.e.

$$u(\theta, t) \approx A_{k_c} e^{\omega_{k_c} t} \sin(k_c \theta). \tag{2.39}$$

Using (2.32) for a large value of y (which is equivalent to small A_{k_c}) we see that to the order of $O(A_{k_c}^2)$ (2.39) can be represented as a sum over $L/2\nu$ poles arranged periodically along the θ axis. Other unstable modes will contribute similar arrays of poles but at much higher values of y, since their amplitude is exponentially smaller. In addition we have nonlinear corrections to the identification of the modes in terms of poles. These corrections can be again expanded in terms of Fourier modes, and again identified with poles, which will be further away along the y axis, and with higher frequencies. To see this one can use (2.35), subtract from $u_p(\theta)$ the leading pole representations, and reexpand in Fourier series. Then we identify the leading order with double the number of poles that are situated twice further away along the y axis.

We note that even when all the unstable modes are present, the number of poles in the first order identification is finite for finite L, since there are only L/ν unstable modes. Counting the number of poles that each mode introduces we get a total number of $(L/\nu)^2$ poles. The number $L/2\nu$ of poles which are associated with the most unstable mode is precisely the number allowed in the stable stationary solution, cf. (2.10). When the poles approach the real axis and cusps begin to develop, the linear analysis no longer holds, but the pole description does.

We now describe the qualitative scenario for the establishment of the steady state. Firstly, we understand that all the poles that belong to less unstable modes will be pushed towards infinity. To see this think of the system at this stage as an array of uncoupled systems with a scale of the order of unity. Each such system will have a characteristic value of y. As we discussed before poles that are further away along the y axis will be pushed to infinity. Therefore the system will remain with the $L/2\nu$ poles of the most unstable mode. The net effect of the poles belonging to the (nonlinearly) stable modes is to destroy the otherwise perfect periodicity of the poles of the unstable mode. The see the effect of the higher order correction to the pole identification we again recall that they can be represented as further away poles with higher frequencies, whose dynamics is similar to the less unstable modes that were just discussed. They do not become more relevant when time goes on.

Once the poles of the stable modes get sufficiently far from the real axis, the dynamics of the remaining poles will begin to develop according to the interactions that are directed along the real axis. These interactions are much weaker and the resulting dynamics occur on much longer time scales. The qualitative picture is of an inverse cascade of merging the θ positions of the poles. We note that the system has a set of unstable fixed points which are 'cellular solutions' described by a periodic

arrangement of poles along the real axis with a frequency k. These fixed points are not stable and they collapse, under perturbations, with a characteristic time scale (that depends on k) to the next unstable fixed point at $k' = k/2$. This process then goes on indefinitely until $k \sim 1/L$ i.e. we reach the giant cusp, the steady-state stable solution [91].

This scenario is seen very clearly in the numerical simulations. In Fig. 2.3, we show the time evolution of the premixed flame front starting from small white-noise initial conditions. The bottom curve pertains to the earliest time in this picture, just after the fast exponential growth, and one sees clearly the periodic array of cusps that form. The successive images show the progress of the premixed flame front in time, and one observes the development of larger scales with deeper cusps that represent the partial coalescence of poles onto the same θ positions. In Fig. 2.4, we show the width and the velocity of this front as a function of time. One recognizes the exponential stage of growth in which the $L/2\nu$ poles approach the θ axis, and then a clear cross-over to much slower dynamics in which the effective scale in the system grows with a slower rate.

The slow dynamics stage can be understood qualitatively using the previous interpretation of the cascade as follows: if the initial number of poles belonging to the unstable mode is $L/2\nu$, the initial effective linear scale is 2ν. Thus the first step of the inverse cascade will be completed in a time scale of the order of 2ν. At this point the effective linear scale doubles to 4ν, and the second step will be completed after such a time scale. We want to know what is the

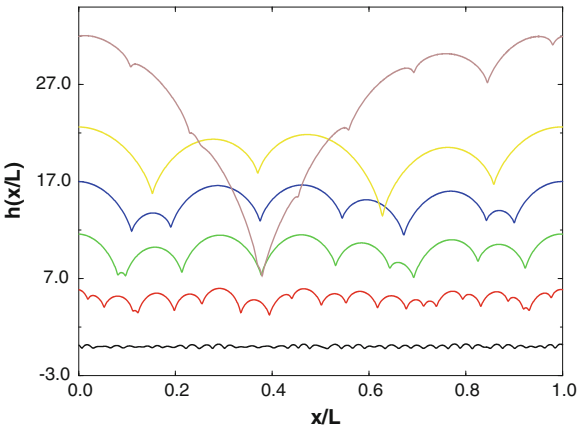

Fig. 2.3 The inverse cascade process of coarsening that occurs after preparing the system with random, small initial conditions. One sees that at successive times the typical scale increases until the giant cusp forms, and attracts all the other side-poles. The effect of the existing numerical additive noise is to introduce poles that appear as side cusp that are continuously attracted to the giant cusp. This effect is obvious to the eye only after the typical scale is sufficiently large, as is seen in the last time (see text for further details)

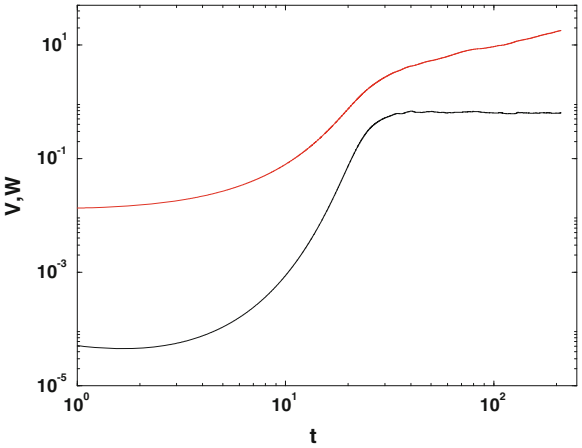

Fig. 2.4 log-log plots of the front velocity (*lower curve)* and width (*upper curve*) as a function of time in the inverse cascade process seen in Fig. 2.3 in a system of size 2000 and $\nu = 1$. Both quantities exhibit an initial exponential growth that turns to a power law growth (after $t \approx 30$). The velocity is constant after this time, and the width increases like t^{ζ}. Note that at the earliest time there is a slight decrease in the velocity; this is due to the decay of linearly stable modes that exist in random initial conditions

typical length scale l_t seen in the system at time t. The definition of front width is $l_t = \sqrt{\frac{1}{\tilde{L}} \int_0^{\tilde{L}} [h(x,t) - \bar{h}]^2 dx}, \bar{h} = \frac{1}{\tilde{L}} \int_0^{\tilde{L}} h(x,t) dx$. The typical width of the system at this stage will be proportional to this scale.

Denote the number of cascade steps that took place until this scale is achieved by s_l. The total time elapsed, $t(l_t)$ is the sum

$$t(l_t) \sim \sum_{i=1}^{s_l} 2^i. \tag{2.40}$$

The geometric sum is dominated by the largest term and we therefore estimate $t(l_t) \sim l_t$. We conclude that the scale and the width are linear in the time elapsed from the initial conditions ($l_t \sim t^{\zeta}$, $\zeta = 1$). In noiseless simulations we find (see Fig. 2.4) a value of ζ which is $\zeta \approx 0.95 \pm 0.1$.

2.4.3 *Inverse Cascade in the Presence of Noise*

An interesting consequence of the discussion in the last section is that the inverse cascade process is an effective "clock" that measures the typical time scales in this system. For future purposes we need to know the typical time scales when the dynamics is perturbed by random noise. To this aim we ran simulations following the inverse

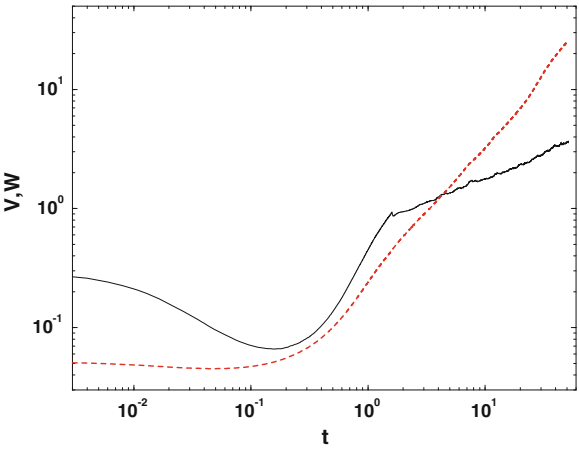

Fig. 2.5 The same as Fig. 2.4 but with additive random noise for a system of size 1000, $\nu = 0.1$ and $f = 10^{-13}$. The velocity does not saturate now, and the exponent ζ characterizing the increase of the width with time changes to $\zeta = 1.2 \pm 0.1$. The velocity increases in time like t^{γ} with $\gamma \approx 0.48 \pm 0.04$

cascade in the *presence* of external noise. The main result that will be used in later arguments is that now the appearance of a typical scale l_t occurs not after time t, but rather according to

$$l_t \sim t^{\zeta}, \quad \zeta \approx 1.2 \pm 0.1. \tag{2.41}$$

The numerical confirmation of this law is exhibited in Fig. 2.5.

We also find that the front velocity in this case increases with time according to

$$v \sim t^{\gamma}, \quad \gamma \approx 0.48 \pm 0.05. \tag{2.42}$$

This result will be related to the acceleration of the premixed flame front in noisy simulations, as will be seen in the next sections.

2.5 Acceleration of the Premixed Flame Front, Pole Dynamics and Noise

A major motivation of this section is the observation that in radial geometry the same equation of motion shows an acceleration of the premixed flame front. The aim of this section is to argue that this phenomenon is caused by the noisy generation of new poles. Moreover, it is our contention that a great deal can be learned about the acceleration in radial geometry by considering the effect of noise in channel growth. In [48] it was shown that any initial condition which is represented in poles goes to a unique stationary state which is the giant cusp which propagates with a constant velocity $v = 1/2$ up to small $1/L$ corrections. In light of our discussion of the last section we expect that any smooth enough initial condition will go to the

same stationary state. Thus if there is no noise in the dynamics of a finite channel, no acceleration of the premixed flame front is possible. What happens if we add noise to the system?

For concreteness we introduce an additive white-noise term $\eta(\theta, t)$to the equation of motion (2.5) where

$$\eta(\theta, t) = \sum_k \eta_k(t) \exp(ik\theta), \tag{2.43}$$

and the Fourier amplitudes η_k are correlated according to

$$\langle \eta_k(t)\eta^*_{k'}(t')\rangle = \frac{f}{L}\delta_{k,k'}\delta(t-t'). \tag{2.44}$$

We will first examine the result of numerical simulations of noise-driven dynamics, and later return to the theoretical analysis.

2.5.1 Noisy Simulations

Initial numerical investigations [46, 86] did not introduce noise in a controlled fashion. We will argue later that some of the phenomena encountered in these simulations can be ascribed to the (uncontrolled) numerical noise. We performed numerical simulations of (2.5) using a pseudo-spectral method. The time-stepping scheme was chosen as Adams-Bashforth with 2nd order precision in time. The additive white noise was generated in Fourier-space by choosing η_k for every k from a flat distribution in the interval $[-\sqrt{2\frac{f}{L}}, \sqrt{2\frac{f}{L}}]$. We examined the average steady state velocity of the front as a function of L for fixed f and as a function of f for fixed L. We found the interesting phenomena that are summarized here:

1. In Fig. 2.6 we can see two different regimes of the behavior of the average velocity v as a function of the noise amplitude $f^{0.5}$ for the fixed system size L. For the noise f smaller then same fixed value f_{cr}

$$v \sim f^{\xi}. \tag{2.45}$$

   For these values of f this dependence is very weak, and $\xi \approx 0.02$. For the large values of f the dependence is much stronger.
2. In Fig. 2.7 we can see the growth of the average velocity v as a function of the system size L. After some values of L we can see saturation of the velocity. For regime $f < f_{cr}$ the growth of the velocity can be written as

$$v \sim L^{\mu}, \quad \mu \approx 0.35 \pm 0.03. \tag{2.46}$$

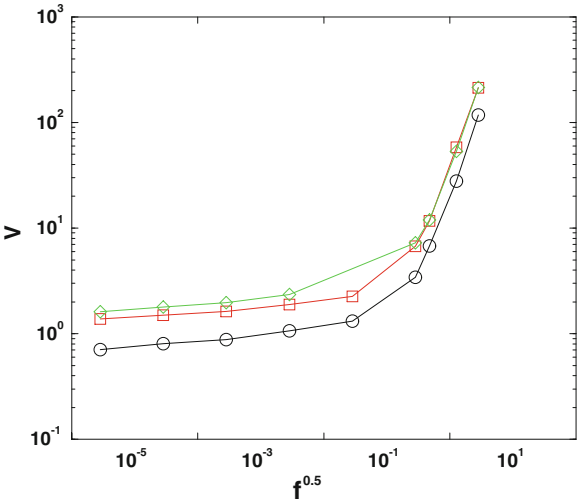

Fig. 2.6 The dependence of the average velocity v on the noise amplitude $f^{0.5}$ for L=10, 40, 80

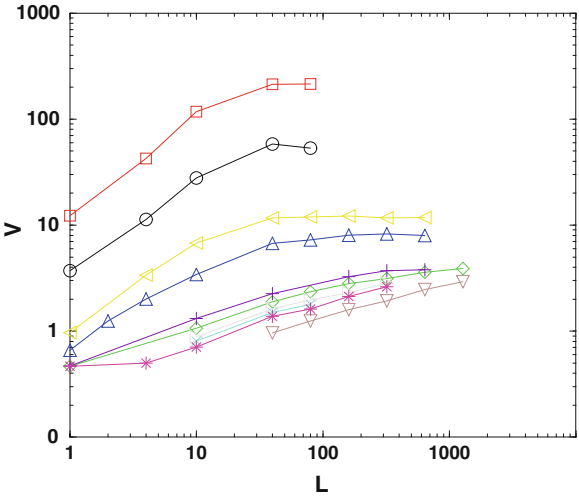

Fig. 2.7 The dependence of the average velocity v on the system size L for noise amplitude $f^{0.5} = 0, 2.7 \times 10^{-6}, 2.7 \times 10^{-5}, 2.7 \times 10^{-4}, 2.7 \times 10^{-3}, 2.7 \times 10^{-2}, 2.7 \times 10^{-1}, 0.5, 1.3, 2.7$

3. In Figs. 2.8 and 2.9 we can see premixed flame fronts for $f < f_{cr}$ and $f > f_{cr}$. For $f > f_{cr}$ in Fig. 2.9 we see qualitative change in the appearance of the premixed flame front: the noise introduces significant levels of small scales structure in addition to the cusps. The same observation was made in [88]: "It is tempting, as some authors have indeed done [27], to identify the effect of noise as generating spurious poles accounting for the appearance and motion of secondary wrinkles on the flame as in (Fig. 11a of [88]). However, such a picture does not seem to fully explain the fractalization of the flame at higher intensities f and higher $(4\pi L)/\nu$ and attempts have thus far failed at generalizing this idea rigorously."

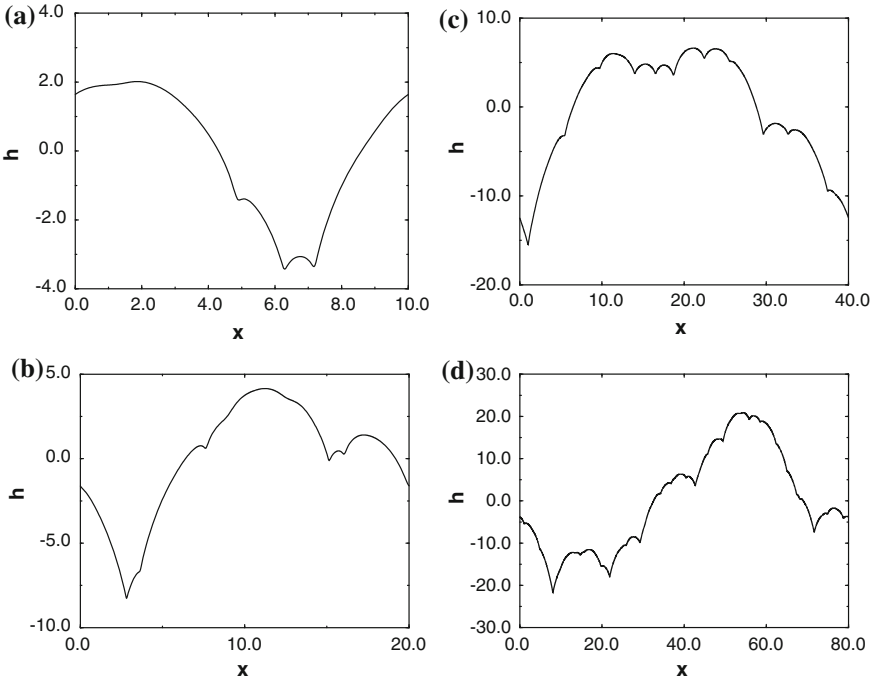

Fig. 2.8 Typical premixed flame fronts for $f < f_{cr}$ where the system is sufficiently small not to be terribly affected by the noise. The effect of noise in this regime is to add additional small cusps to the giant cusp. In figures a-d we present fronts for growing system sizes $\tilde{L} = 10, 20, 40$ and 80 respectively, $\nu = 0.1$. One can observe that when the system size grows there are more cusps with a more complex structure

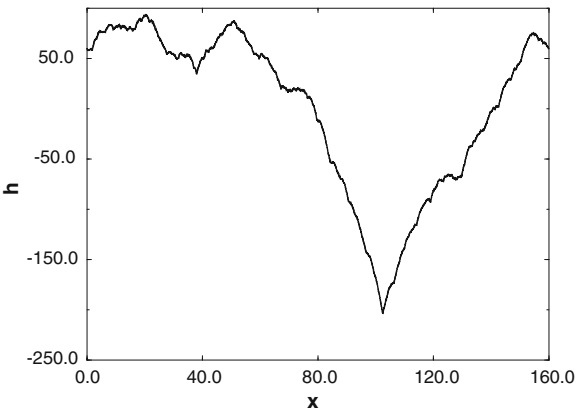

Fig. 2.9 A typical premixed flame front for $f > f_{cr}$. The system size is 160. This is sufficient to cause a qualitative change in the appearance of the premixed flame. *Front* The noise introduces significant levels of small scales structure in addition to the cusps

2.5.2 Calculation of the Number of Poles in the System

The interesting problem that we would like to solve here to better understand the dynamics of poles, is to determine those that exist in our system outside the giant cusp. This can be done by calculating the number of cusps (points of minimum or inflectional points) and their position on the interval $\theta : [0, 2\pi]$ in every moment of time and drawing the positions of the cusps like functions of time, see Fig. 2.10. In this picture we can see the x-positions of all cusps in the system as a function of time.

We have assumed that our system is in a "quasi-stable" state most of the time, i.e. every new cusp that appears in the system includes only one pole. Using pictures obtained in this way we can find:

1. The mean number of poles in the system. By calculating the number of cusps in some moment of time and by investigating the history of every cusp (except the giant cusp), i.e. how many initial cusp take part in formatting this cusp, and after averaging the number of poles found with respect to different moments of time, we can find the mean number of poles that exist in our system outside the giant cusp. Let us denote this number by δN. There are four regimes that can be defined with respect to the dependence of this number on the noise f: (i) Regime I: Such little noise that no new cusp exist in our system outside the giant cusp; (ii) Regime II: Strong dependence of the pole number δN on the noise f; (iii) Regime III: Saturation of the pole number δN on the noise f, so that this number depends very little on the noise (Fig. 2.11);

$$\delta N \sim f^{0.03} \tag{2.47}$$

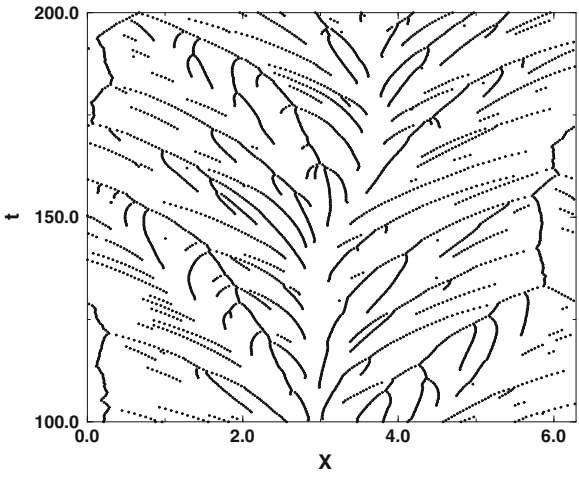

Fig. 2.10 The dependence of the cusps positions on time. $L = 80\ \nu = 0.1$ $f = 9 \times 10^{-6}$

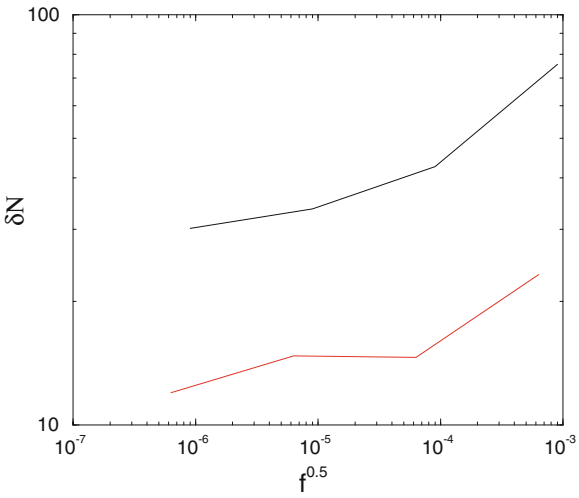

Fig. 2.11 The dependence of the excess pole number δN on the noise amplitude $f^{0.5}$. $\nu = 0.1$ $L = 40, 80$

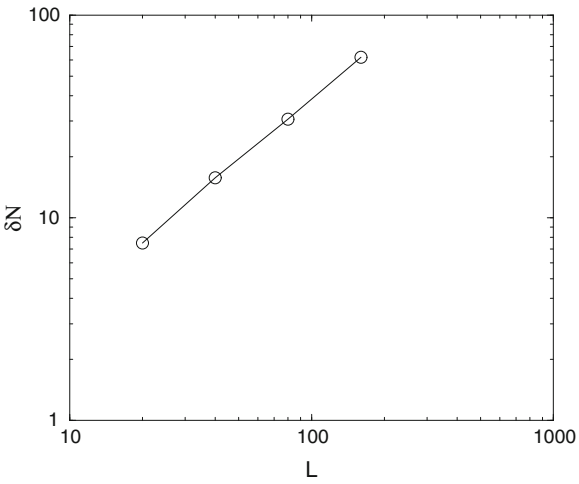

Fig. 2.12 The dependence of the excess pole number δN on the system size L. $\nu = 0.1$ $f^{0.5} = 9 \times 10^{-6}$

The saturated value of δN is defined by next formula (Figs. 2.12 and 2.13)

$$\delta N \approx N(L)/2 \approx \frac{1}{4}\frac{L}{\nu} \tag{2.48}$$

where $N(L) \approx \frac{1}{2}\frac{L}{\nu}$ is the number of poles in the giant cusp. (iv) Regime IV: We again see a strong dependence of the pole number δN on the noise f (Fig. 2.11);

$$\delta N \sim f^{0.1} \tag{2.49}$$

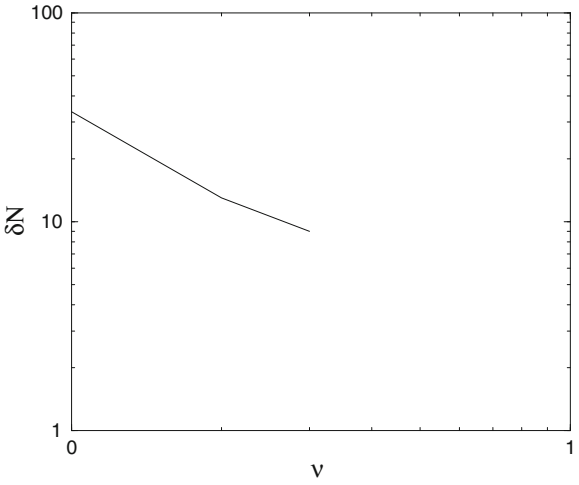

Fig. 2.13 The dependence of the excess pole number δN on the parameter ν. $L = 80$ $\nu = 0.1$

Because of the numerical noise we can see in most of the simulations only regime III and IV. In the future if no new evidence is seen we will discuss regime III.

2. We suppose that any new *cusp* (that appear in the system) corresponds to new *pole*. So, by calculating the new *cusp* number that appears in the system in the unit time we can find the number of new *poles* that appear in the system in the unit time $\frac{dN}{dt}$. In regime III (Fig. 2.14).

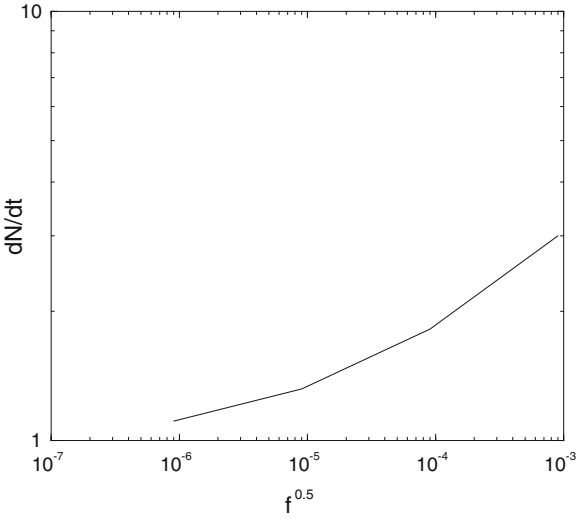

Fig. 2.14 The dependence of the pole number in the unit time dN/dt on the noise amplitude $f^{0.5}$. $\nu = 0.1$ $L = 80$

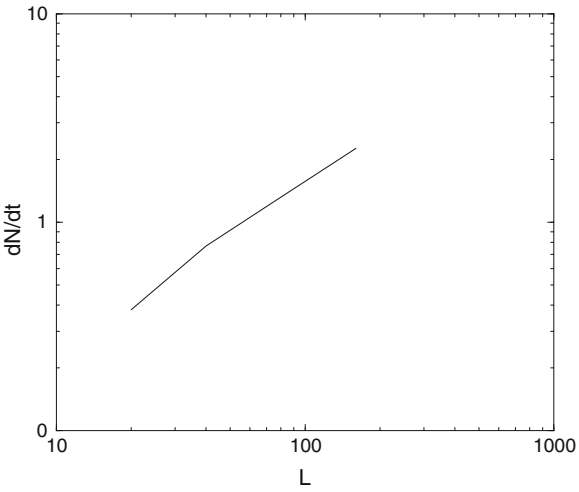

Fig. 2.15 The dependence of the pole number in the unit time dN/dt on the system size L. $\nu = 0.1$ $f^{0.5} = 9 \times 10^{-6}$

$$\frac{dN}{dt} \sim f^{0.03} \tag{2.50}$$

The dependence on L and ν is defined by (Figs. 2.15 and 2.16)

$$\frac{dN}{dt} \sim L^{0.8} \tag{2.51}$$

$$\frac{dN}{dt} \sim \frac{1}{\nu^2} \tag{2.52}$$

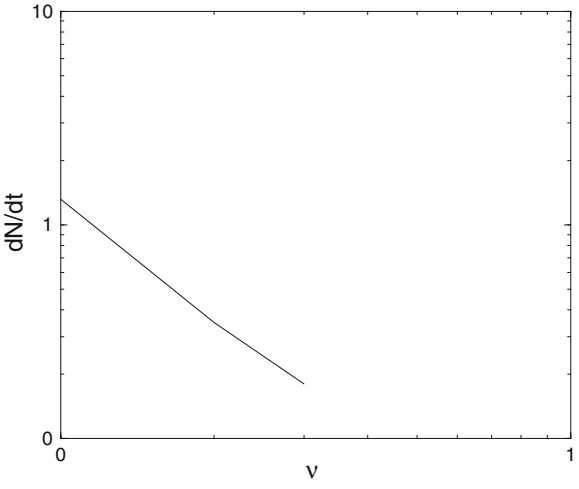

Fig. 2.16 The dependence of the pole number in the unit time dN/dt on the parameter ν. $L = 80$ $\nu = 0.1$

In regime IV, the dependence on the noise is defined by the following: (Fig. 2.14)

$$\frac{dN}{dt} \sim f^{0.1} \tag{2.53}$$

2.5.3 *Theoretical Discussion of the Effect of Noise*

2.5.3.1 The Threshold of Instability to Added Noise. Transition from Regime I to Regime II

First we present the theoretical arguments that explain the sensitivity of the giant cusp giant cusp solution to the effect of added noise. This sensitivity increases dramatically with increasing the system size L. To see this we use again the relationship between the linear stability analysis and the pole dynamics. Our additive noise introduces perturbations with all k-vectors. We showed previously that the most unstable mode is the $k = 1$ component $A_1 \sin(\theta)$. Thus the most effective noisy perturbation is $\eta_1 \sin(\theta)$ which can potentially lead to a growth of the most unstable mode. Whether or not this mode will grow depends on the amplitude of the noise. To see this clearly we return to the pole description. For small values of the amplitude A_1 we represent $A_1 \sin(\theta)$ as a single pole solution of the functional form $\nu e^{-y} \sin\theta$. The y position is determined from $y = -\log|A_1|/\nu$, and the θ-position is $\theta = \pi$ for positive A_1 and $\theta = 0$ for negative A_1. From the analysis of Sect. 2.3 we know that for very small A_1 the fate of the pole is to be pushed to infinity, independently of its θ position; the dynamics is symmetric in $A_1 \to -A_1$ when y is large enough. On the other hand when the value of A_1 increases the symmetry is broken and the θ position and the sign of A_1 become very important. If $A_1 > 0$ there is a threshold value of y below which the pole is attracted down. On the other hand if $A_1 < 0$, and $\theta = 0$ the repulsion from the poles of the giant cusp grows with decreasing y. We thus understand that qualitatively speaking the dynamics of A_1 is characterized by an asymmetric "potential" according to

$$\dot{A}_1 = -\frac{\partial V(A_1)}{\partial A_1}, \tag{2.54}$$

$$V(A_1) = \lambda A_1^2 - a A_1^3 + \cdots \tag{2.55}$$

From the linear stability analysis we know that $\lambda \approx \nu/L^2$, cf. (2.11). We know further that the threshold for nonlinear instability is at $A_1 \approx \nu^3/L^2$, cf. (2.26). This determines that value of the coefficient $a \approx 2/3\nu^2$ (This value corresponds to maximum of $V(A_1)$ and zero-force). The magnitude of the "potential" at the maximum is

$$V(A_{max}) \approx \nu^7/L^6. \tag{2.56}$$

The effect of the noise on the development of the mode $A_1 \sin\theta$ can be understood from the following stochastic equation

$$\dot{A}_1 = -\frac{\partial V(A_1)}{\partial A_1} + \eta_1(t). \tag{2.57}$$

It is well known [92] that for such dynamics the rate of escape R over the "potential" barrier for small noise is proportional to

$$R \sim \frac{\nu}{L^2} \exp^{-\nu^7/fL^5}. \tag{2.58}$$

The conclusion is that any arbitrarily tiny noise becomes effective when the system size increase and when ν decreases. If we drive the system with noise of amplitude $\frac{f}{L}$ the system can always be sensitive to this noise when its size exceeds a critical value L_c that is determined by $f/L_c \sim \nu^7/L_c^6$. This formula defines transition from regime I (no new cusps) to regime II. For $L > L_c$ the noise will introduce new poles into the system. Even numerical noise in simulations involving large size systems may have a macroscopic influence.

The appearance of new poles must increase the velocity of the front. The velocity is proportional to the mean of $(u/L)^2$. New poles distort the giant cusp by additional smaller cusp on the wings of the giant cusp, increasing u^2. Upon increasing the noise amplitude more and more smaller cusp appear in the front, and inevitably the velocity increases. This phenomenon is discussed quantitatively in Sect. 2.5.

2.5.3.2 Numerical Verifying of the Asymmetric "potential": Form and Dependence of the Noise on L_c

From the equations of the motion for poles (see (2.10)–(2.12)) we can find the distribution of poles in the giant cusp [48]. If we know the distribution of poles in the giant cusp we can then find the form of the "potential" and verify numerically expressions for values λ, A_{max} and $\frac{\partial V(A_1)}{\partial A_1}$ discussed previously. The connection between amplitude A_1 and the position of the pole y is defined by $A_1 = 4\nu e^{-y}$ and the connection between the potential function $\frac{\partial V(A_1)}{\partial A_1}$ and the position of the pole y is defined by formula $\frac{\partial V(A_1)}{\partial A_1} = 4\nu \frac{dy}{dt} e^{-y}$, where $\frac{dy}{dt}$ can be determined from the equation of the motion of the poles. We can find A_{max} as the zero-point of $\frac{\partial V(A_1)}{\partial A_1}$ and λ can be found as $\frac{1}{2}\frac{\partial^2 V(A_1)}{\partial A_1^2}$ for $A_1 = 0$. Numerical measurements were made for the set of values $L = 2n\nu$, where n is a integer and $n > 2$. For our numerical measurements we use the constant $\nu = 0.005$ and the variable L, where L changes in the interval [1, 150], or variable ν that changes in the interval [0.005, 0.05] and the constant $L = 1$. The results obtained follow:

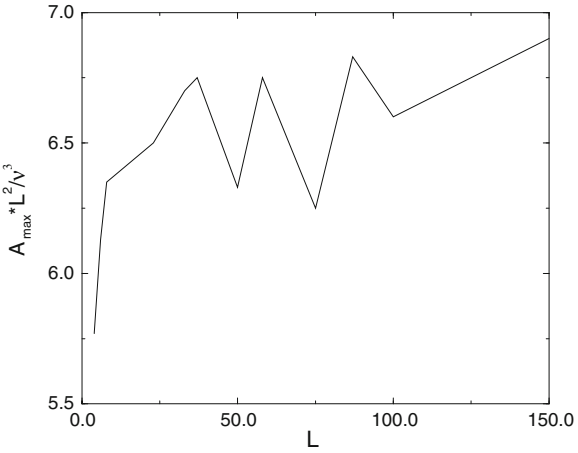

Fig. 2.17 The dependence of the normalized amplitude $A_{max}L^2/\nu^3$ on the system size L

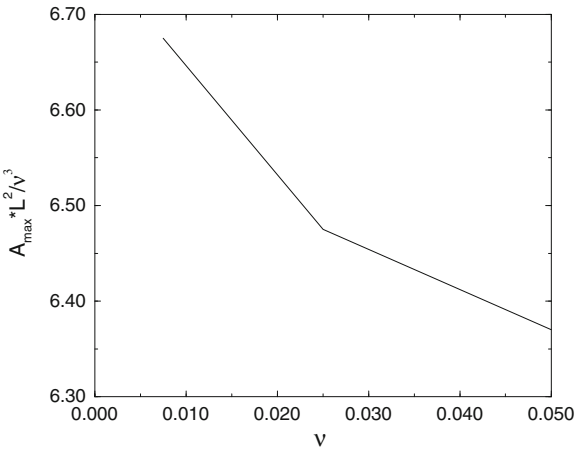

Fig. 2.18 The dependence of the normalized amplitude $A_{max}L^2/\nu^3$ on the parameter ν

1. $\frac{A_{max}L^2}{\nu^3}$ as a function of L is almost a constant (Fig. 2.17).
2. $\frac{A_{max}L^2}{\nu^3}$ as a function of ν is almost a constant (Fig. 2.18).
3. $\frac{A_{max}}{A_{N(L)}}$ as a function of L is almost a constant. $A_{N(L)}$ is defined by the position of the upper pole (Fig. 2.19).
4. $\frac{A_{max}}{A_{N(L)}}$ as a function of ν is almost a constant (Fig. 2.20).
5. The value of $\frac{\lambda L^2}{\nu}$ as a function of L is a constant (Fig. 2.21).
6. The value of $\frac{\lambda L^2}{\nu}$ as a function of ν is a constant (Fig. 2.22).

We also verify the boundary between regime I (no new cusp) and regime II (new cusp appear). Figure 2.23 shows the dependence of $\frac{f}{L_c}$ on L_c. We can see that $f/L_c \sim 1/L_c^6$. These results are in good agreement with the theory.

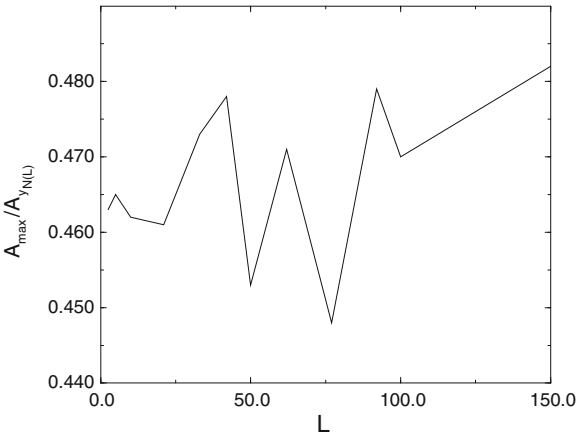

Fig. 2.19 The relationship between the amplitude defined by the minimum of the potential A_{max} and the amplitude defined by the position of the *upper* pole $A_{N(L)}$ as a function of the system size L

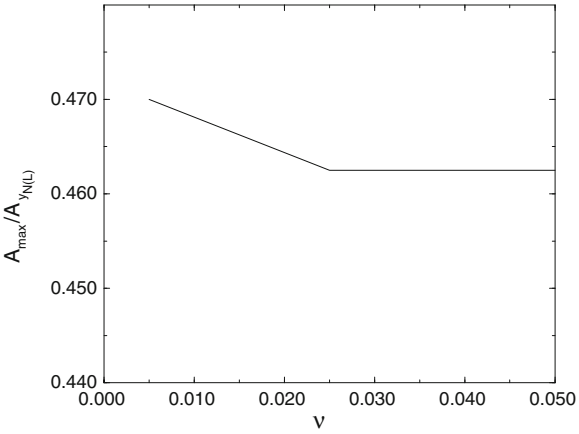

Fig. 2.20 The relationship between the amplitude defined by the minimum of the potential A_{max} and the amplitude defined by the position of the *upper* pole $A_{N(L)}$ as a function of the parameter ν

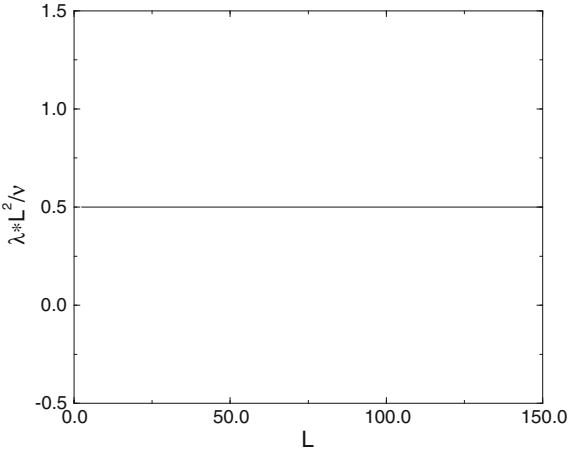

Fig. 2.21 The dependence of the normalized parameter $\lambda L^2/\nu$ on the system size L

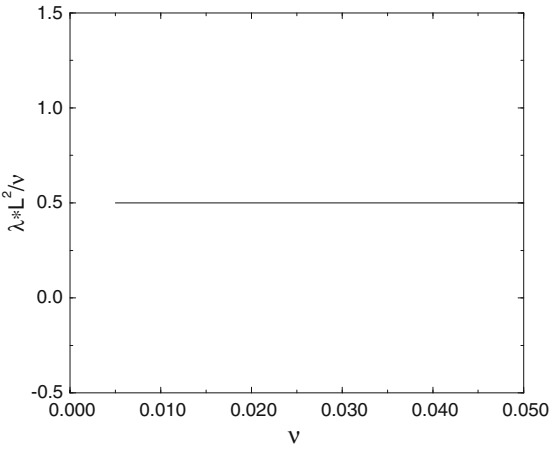

Fig. 2.22 The dependence of the normalized parameter $\lambda L^2/\nu$ on the parameter ν

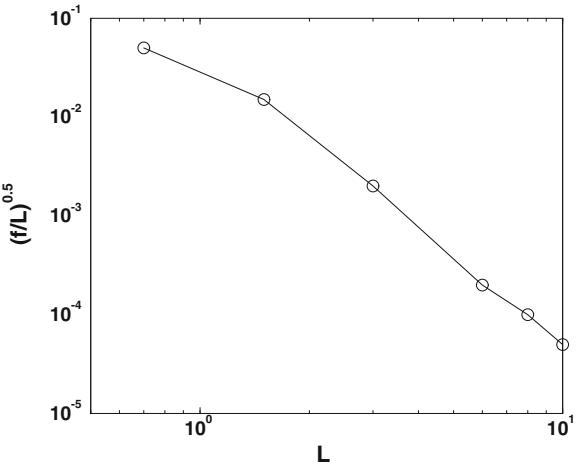

Fig. 2.23 The dependence of the critical noise on the system size

2.5.3.3 The Noisy Steady State and Its Collapse with Large Noise and System Size

In this subsection we discuss the response of the giant cusp solution to noise levels that are able to introduce a large number of excess poles in addition to those existing in the giant cusp. We will denote the excess number of poles by δN. The first question that we address is how difficult is it to insert yet an additional pole when there is already a given excess δN. To this aim we estimate the effective potential $V_{\delta N}(A_1)$ which is similar to (2.55) but is taking into account the existence of an excess number of poles. A basic approximation that we employ is that the fundamental form of the giant cusp solution is not seriously modified by the existence of an excess number of poles. Of course this approximation breaks down quantitatively already with one

excess pole. Qualitatively however it holds well until the excess number of poles is of the order of the original number $N(L)$ of the giant cusp solution. Another approximation is that the rest of the linear modes play no role in this case. At this point we limit the discussion therefore to the situation $\delta N \ll N(L)$ (regime II).

To estimate the parameter λ in the effective potential we consider the dynamics of one pole whose y position y_a is far above y_{max}. According to (2.11) the dynamics reads

$$\frac{dy_a}{dt} \approx \frac{2\nu(N(L)+\delta N)}{L^2} - \frac{1}{L} \tag{2.59}$$

Since the $N(L)$ term cancels against the L^{-1} term Eq. (1.10), we remain with a repulsive term that in the effective potential translates to

$$\lambda = \frac{\nu \delta N}{L^2}. \tag{2.60}$$

Next we estimate the value of the potential at the break-even point between attraction and repulsion. In the last subsection we saw that a foreign pole has to be inserted below y_{max} in order to be attracted towards the real axis. Now we need to push the new pole below the position of the existing pole whose index is $N(L) - \delta N$. This position is estimated as in Sect. 2.3.4 by employing the TFH distribution function (2.23). We find

$$y_{\delta N} \approx 2 \ln \left[\frac{4L}{\pi^2 \nu \delta N} \right]. \tag{2.61}$$

As before, this implies a threshold value of the amplitude of single pole solution $A_{max} \sin\theta$ which is obtained from equating $A_{max} = \nu e^{-y_{\delta N}}$. We thus find in the present case $A_{max} \sim \nu^3 (\delta N)^2 / L^2$. Using again a cubic representation for the effective potential we find $a = 2/(3\nu^2 \delta N)$ and

$$V(A_{max}) = \frac{1}{3} \frac{\nu^7 (\delta N)^5}{L^6}. \tag{2.62}$$

Repeating the calculation of the escape rate over the potential barrier we find in the present case

$$R \sim \frac{\nu \delta N}{L^2} \exp^{-\nu^7 (\delta N)^5 / f L^5}. \tag{2.63}$$

For a given noise amplitude f there is always a value of L and ν for which the escape rate is of $O(1)$ as long as δN is not too large. When δN increases the escape rate decreases, and eventually no additional poles can creep into the system. The typical number δN for fixed values of the parameters is estimated from equating the argument in the exponent to unity

$$\delta N \approx \left(fL^5/\nu^7\right)^{1/5}. \tag{2.64}$$

We can see that δN is strongly dependent on noise f, in contrast to regime III. Let us find the conditions of transition from regime II to III, where we see the saturation of δN with respect to noise f.

(i) We use the expression $A_{max} = 4\nu e^{-y_{\delta N}}$ for the amplitude of the pole solution that equals to $\frac{2\nu \sin\theta}{\cosh(y_{\delta N}) - \cos\theta}$; however, this is correct only for the large number $y_{\delta N}$. When $y_{\delta N} < 1$, a better approximation is $A_{max} = \frac{4\nu}{y_{\delta N}^2}$. From the (2.61) we find that the boundary value $y_{\delta N} = 1$ corresponds to $\delta N \approx N(L)/2$.

(ii) We use the expression $y_{\delta N} \approx 2\ln\left[\frac{4L}{\pi^2\nu\delta N}\right]$, but for a large value of δN a better approximation that can be found the same way is $y_{\delta N} \approx \frac{\pi^2\nu}{2L}(N(L) - \delta N)\ln\left[\frac{8eL}{\pi^2\nu(N(L)-\delta N)}\right]$ [48]. These expressions give us nearly the same result for $\delta N \approx N(L)/2$.

From (i) and (ii) we can make the following conclusions:

(a) The transition from regime II to regime III generally occurs for $\delta N \approx N(L)/2$;

(b) Using the new expressions in (i) and (ii) for the amplitude A_{max} and $y_{\delta N}$, we can determine the noise $\frac{f}{L}$ in regime III by

$$\frac{f}{L} \sim V(A_{max}) \sim \lambda A_{max}^2 \sim \frac{\nu\delta N}{L^2}\left(\frac{4\nu}{y_{\delta N}^2}\right)^2 \sim \frac{L^2}{\nu}\frac{\delta N}{(N(L) - \delta N)^4} \tag{2.65}$$

This expression defines a very slight dependence of δN on the noise f for $\delta N > N(L)/2$, which explains the noise saturation of δN for regime III.

(c) The form of the giant cusp solution is governed by the poles that are close to zero with respect to y. For the regime III, $N(L)/2$ poles that have positions $y < y_{\delta N = N(L)/2} = 1$ remain at this position. This result explains why the giantcusp solution cannot be seriously modified for regime III.

From (2.64) by using the condition

$$\delta N \approx N(L)/2 \tag{2.66}$$

the boundary noise f_b between regimes II and III can be found as

$$f_b \sim \nu^2. \tag{2.67}$$

The basic equation describing pole dynamics follows

$$\frac{dN}{dt} = \frac{\delta N}{T}, \tag{2.68}$$

where $\frac{dN}{dt}$ is the number of poles that appear in the unit time in our system, δN is the excess number of poles, and T is the mean lifetime of a pole (between appearing

and merging with the giant cusp). Using the result of numerical simulations for $\frac{dN}{dt}$ and (2.66) we can find for T

$$T = \frac{\delta N}{\frac{dN}{dt}} \sim \nu L^{0.2}. \tag{2.69}$$

Thus the lifetime is proportional to ν and depends on the system size L very slightly.

Moreover, the lifetime of a pole is defined by the lifetime of the poles that are in a cusp. From the maximum point of the linear part of (2.1), we can find the mean character size (the same result was gotten in [67], see Fig. 9 in [67])

$$\lambda_m \sim \nu \tag{2.70}$$

that defines the size of our cusp. The mean number of poles in a cusp

$$n_{big} \approx \frac{\lambda_m}{2\nu} \sim const \tag{2.71}$$

does not depend on L and ν. The mean number of cusp is

$$N_{big} \sim \frac{\delta N}{n_{big}} \sim \frac{L}{\nu}. \tag{2.72}$$

Let us assume that some cusp exists in the main minimum of the system. The lifetime of a pole in such a cusp is defined by three parts.

(I) Time of the cusp formation. This time is proportional to the cusp size (with ln-corrections) and the pole number in the cusp (from pole motion equations)

$$T_1 \sim \lambda_m n_{big} \sim \nu \tag{2.73}$$

(II) Time that the cusp is in the minimum neighborhood. This time is defined by

$$T_2 \sim \frac{a}{v} \tag{2.74}$$

where a is a neighborhood of minimum, such that the force from the giant cusp is smaller than the force from the fluctuations of the excess pole number δN, and v is the velocity of a pole in this neighborhood. Fluctuations of excess pole number δN are expressed as

$$N_{fl} = \sqrt{\delta N}. \tag{2.75}$$

From this result and the pole motion equations we find that

$$v \sim \frac{\nu}{L} N_{fl} \sim \frac{\nu}{L}\sqrt{\frac{L}{\nu}} \sim \sqrt{\frac{\nu}{L}}. \tag{2.76}$$

The velocity from the giant cusp is defined by

$$v \sim \frac{\nu}{L} N(L) \frac{a}{L} \sim \frac{a}{L}. \tag{2.77}$$

So from equating these two equations we obtain

$$a \sim \sqrt{\nu L}. \tag{2.78}$$

Thus for T_2 we obtain

$$T_2 \sim \frac{a}{v} \sim L. \tag{2.79}$$

(III) Time of attraction to the giant cusp. From the equations of motion for the poles we get

$$T_3 \sim L \ln(\frac{L}{a}) \sim L \ln \sqrt{L} \sim L. \tag{2.80}$$

For the domain of the system sizes, which was investigated numerically above, we can conclude from (2.69):

$$T_1 \gg T_2, T_3 \tag{2.81}$$

Therefore full lifetime is

$$T = T_1 + T_2 + T_3 \sim \nu + sL, \tag{2.82}$$

where s is a constant and

$$0 < s \ll 1. \tag{2.83}$$

This result qualitatively and partly quantatively explains dependence (2.69). From (2.66), (2.68), (2.69) we can see that in regime III $\frac{dN}{dt}$ is saturated with the system size L.

2.5.4 *The Acceleration of the Premixed Flame Front Because of Noise*

In this section we estimate the scaling exponents that characterize the velocity of the premixed flame front as a function of the system size. To estimate the velocity of the

premixed flame front we need to create an equation for the mean of $\langle dh/dt \rangle$ given an arbitrary number N of poles in the system. This equation follows directly from (2.4)

$$\left\langle \frac{dh}{dt} \right\rangle = \frac{1}{L^2} \frac{1}{2\pi} \int_0^{2\pi} u^2 d\theta. \tag{2.84}$$

After substitution of (2.8) in (2.84) we get, using (2.11) and (2.12)

$$\left\langle \frac{dh}{dt} \right\rangle = 2\nu \sum_{k=1}^{N} \frac{dy_k}{dt} + 2\left(\frac{\nu N}{L} - \frac{\nu^2 N^2}{L^2} \right). \tag{2.85}$$

Estimating the second and third terms in this equation are straightforward. Writing $N = N(L) + \delta N(L)$ and remembering that $N(L) \sim L/\nu$ and $\delta N(L) \sim N(L)/2$, we find that these terms contribute $O(1)$. The first term contributes only when the current of the poles is asymmetric. Noise introduces poles at a finite value of y_{min}, whereas the rejected poles stream towards infinity and disappear at the boundary of nonlinearity defined by the position of the highest pole as

$$y_{max} \approx 2 \ln \left[\frac{4L}{\pi^2 \nu} \right]. \tag{2.86}$$

Thus we have an asymmetry that contributes to the velocity of the front. To estimate the first term let us define

$$d\left(\sum \frac{dy_k}{dt} \right) = \sum_{l}^{l+dl} \frac{dy_k}{dt}, \tag{2.87}$$

where $\sum_l^{l+dl} \frac{dy_k}{dt}$ is the sum over the poles that are on the interval $y : [l, l + dl]$. We can write

$$d\left(\sum \frac{dy_k}{dt} \right) = d\left(\sum \frac{dy_k}{dt} \right)_{up} + d\left(\sum \frac{dy_k}{dt} \right)_{down}, \tag{2.88}$$

where $d\left(\sum \frac{dy_k}{dt} \right)_{up}$ is the flux of poles moving up and $d\left(\sum \frac{dy_k}{dt} \right)_{down}$ is the flux of poles moving down.

For these fluxes we can write

$$d\left(\sum \frac{dy_k}{dt} \right)_{up}, -d\left(\sum \frac{dy_k}{dt} \right)_{down} \leq \frac{dN}{dt} dl. \tag{2.89}$$

So for the first term

$$0 \le \sum_{k=1}^{N} \frac{dy_k}{dt} = \int_{y_{min}}^{y_{max}} \frac{d\left(\sum \frac{dy_k}{dt}\right)}{dl} dl \tag{2.90}$$
$$= \int_{y_{min}}^{y_{max}} \frac{d\left(\sum \frac{dy_k}{dt}\right)_{up} + d\left(\sum \frac{dy_k}{dt}\right)_{down}}{dl} dl$$
$$\le \frac{dN}{dt}(y_{max} - y_{min})$$
$$\le \frac{dN}{dt} y_{max}$$

Because of slight (ln) dependence of y_{max} on L and ν, $\frac{dN}{dt}$ term determines order of nonlinearity for the first term in (2.85). This term equals zero for the symmetric current of poles and achieves the maximum for the maximal asymmetric current of poles. A comparison of $v \sim L^{0.35} f^{0.02}$ and $\frac{dN}{dt} \sim L^{0.8} f^{0.03}$ confirms this calculation.

2.6 Comparison with Experiment for Premixed Flame in Channel

The available experimental data clearly indicate that freely expanding wrinkled premixed flame with Darrieus-Landau hydrodynamic instability possess the following intrinsic features in channel:

1. Planar premixed flame front is unstable, becomes weakened by stretch and tulip shape of the premixed flame is formed (the so called "stretch-effect"). The tulip top is pointed to direction of propagation [93–95]. After increasing channel size multi-quasi-cusps (multi-cells) structure of the premixed flame front appears [11, 96, 97] (The premixed flame front consists of a large number of quasi-cusps, i.e., cusps with rounded tips).
2. if the channel size increases then the velocity of the premixed flame front also increases [98–100].

Our numerical investigation corresponds to these experiments.

What can happen if the radius of the channel size growths and its velocity also increases? Either the velocity saturates for big channel sizes (we observe this case in numerical simulations) or transition of the deflagration front into the detonation wave (DDT) appears [101, 102] (DDT can happen if velocity becomes larger than sound velocity or even earlier, because of the other reasons [103]).

2.7 Summary and Conclusions

The main two messages of this chapter are: (i) There is an important interaction between the instability of developing fronts and random noise; (ii) This interaction and its implications can be understood qualitatively and sometimes quantitatively using the description in terms of complex poles.

The pole description is natural in this context firstly because it provides an exact (and effective) representation of the steady state without noise. Once one succeeds to describe also the *perturbations* about this steady state in terms of poles, one achieves a particularly transparent language for the study of the interplay between noise and instability. This language also allows us to describe in qualitative and semi-quantitative terms the inverse cascade process of increasing typical lengths when the system relaxes to the steady state from small, random initial conditions.

The main conceptual steps in this chapter are as follows: firstly one realizes that the steady state solution, which is characterized by $N(L)$ poles aligned along the imaginary axis is marginally stable against noise in a periodic array of L values. For all values of L the steady state is nonlinearly unstable against noise. The main and foremost effect of noise of a given amplitude f is to introduce an excess number of poles $\delta N(L, f)$ into the system. The existence of this excess number of poles is responsible for the additional wrinkling of the premixed flame front on top of the giant cusp, and for the observed acceleration of the premixed flame front. By considering the noisy appearance of new poles we rationalize the observed scaling laws as a function of the noise amplitude and the system size.

The "phase diagram" as a function of L and f in this system consists of four regimes (in [24], which corrects the previous paper [27]). In the first one, discussed in Sect. 2.5.3, the noise is too small to have any effect on the giant cusp solution. The second regime (very small excess number of poles) can not be observed because of numerical noise and discussed only theoretically. In the third regime the noise introduces excess poles that serve to decorate the giant cusp with side cusp. In this regime we find scaling laws for the velocity as a function of L and f and we are reasonably successful in understanding the scaling exponents. In the fourth regime the noise is large enough to create small scale structures that are not neatly understood in terms of individual poles. It appears from our numerics that in this regime the roughening of the premixed flame front gains a contribution from the small scale structure in a way that is reminiscent of *stable*, noise driven growth models like the Kardar-Parisi-Zhang model.

One of our main motivations in this research was to understand the phenomena observed in radial geometry with expanding premixed flame fronts. We note that many of the insights offered above translate immediately to that problem. Indeed, in radial geometry the premixed flame front accelerates and cusps multiply and form a hierarchic structure as time progresses. Since the radius (and the typical scale) increase in this system all the time, new poles will be added to the system even by a vanishingly small noise. The marginal stability found above holds also in this case, and the system will allow the introduction of excess poles as a result of noise.

The results discussed in [28] can be combined with the present insights to provide a theory of radial growth.This theory was offered in [26] (Chap. 4).

We have a serious open problem for this case [104]. For a cylindrical case of the premixed flame front propagation problem at absence of noise (only numerical noise [56–60]) by Sivashinsky with help of numerical methods it was shown, that the premixed flame front is continuously accelerated. During all this account time it is not visible any attributes of saturation. To increase time of the account is a difficult task. Hence, absence or presence of velocity saturation in a cylindrical case of SFF equation [46] is a open problem.

For the best understanding of dependence of premixed flame front velocity as functions of its radius in a cylindrical case similar dependence of premixed flame front velocity on width of the channel (in a flat case) also was analyzed by numerical methods. Growth of velocity is also observed and at absence of noise (only numerical noise!) also any saturation of the velocity it is not observed. Introduction obvious Gaussian noise results to appearance of a point of saturation and its removal from the origin of coordinates with decreasing of noise amplitude, allowing extrapolating results on small numerical noise (Fig. 2.7).

Hence, introducing of Gaussian noise in numerical calculation also for a cylindrical case can again results to appearance of a saturation point and will allow to investigate its behavior as function of noise amplitude by extrapolating results on small numerical noise.

Indeed, Karlin and Sivashinsky [61] informed that the saturation was observed for both 1D and 2D cases in numerical simulations with the noise term of MS and SFF equations. However, in the next paper [62] the authors already suppose not the velocity saturation in 2D case, but stabilization of the acceleration exponent at 1.25.

Finally, the success of this approach in the case of premixed flame propagation raises hope that Laplacian growth patterns may be dealt with using similar ideas. A problem of immediate interest is Laplacian growth in channels, in which a finger steady-state solution is known to exist. It is documented that the stability of such a finger solution to noise decreases rapidly with increasing the channel width. In addition, it is understood that noise brings about additional geometric features on top of the finger. There are enough similarities here to indicate that a careful analysis of the analytic theory may shed as much light on that problem as on the present one.

Appendix: Derivation of Michelson Sivashinsky Equation

In the Appendix we mainly follow to the short derivation of [105]. More detailed derivation of Michelson Sivashinsky equation can be found in [29].

From the hydrodynamic principles of premixed flame propagation, the diffusion length which usually characterizes the premixed flame thickness l_f is thought to be very little if compared to the typical size of the area L. as a result a premixed flame

can be approximated to a surface of infinitesimal width separating the fresh unburnt mixture from the burnt combustion products. Stream on either part of the premixed flame is supposed being inviscid and incompressible, a full detailed description which can be given by the Euler equations

$$\nabla \cdot \mathrm{v} = 0 \tag{2.91}$$
$$\rho \frac{\partial \mathrm{v}}{\partial t} = \rho \left(\nabla \cdot \mathrm{v}\right) \mathrm{v} = -\nabla p$$

in which v is the velocity, p is the pressure and ρ is the density that is piecewise constant, having values ρ_u for the unburnt gas and ρ_b for the burnt gas. A premixed flame surface is mathematically displayed by the function $\psi(x, t)$ provided by

$$\psi(x, t) = y - f(x, t) = 0 \tag{2.92}$$

in which $\psi < 0$ relates to the fresh unburnt mixture and $\psi > 0$ is the burnt mixture. The unit normal vector n to the premixed flame surface provided by $\mathrm{n}=\nabla\psi/|\nabla\psi|$ is directed towards the burnt part. The propagation velocity of the premixed flame surface V_f, normal to itself, is provided by $V_f = -\psi_t/|\nabla\psi|$. Making use of (2.92) the expressions for n and V_f can be written as

$$n = \left(\frac{-f_x}{\sqrt{1+f_x^2}}, \frac{1}{\sqrt{1+f_x^2}}\right) \tag{2.93}$$

$$V_f = \frac{f_t}{\sqrt{1+f_x^2}} \tag{2.94}$$

The flow quantities suffer from jump discontinuities throughout the premixed flame surface and even are subject to the Rankine Hugoniot jump relations given below

$$[[\rho \left(\mathrm{v} \cdot n - V_f\right)]] = 0$$
$$[[n \times (\mathrm{v} \times n)]] = 0 \tag{2.95}$$
$$[[p + \rho \left(\mathrm{v} \cdot n\right) \left(\mathrm{v} \cdot n - V_f\right)]] = 0$$

in which $v = (u, v)$ and $[[.]]$ means the jump in the quantity throughout the premixed flame surface. The premixed flame velocity S_f is described as the propagation velocity of the surface comparably to the incoming unburnt gas, viz. $S_f = \mathrm{v}^* \cdot n - V_f$,

in which $\mathrm{v}^* = \mathrm{v}|_{\psi=0^-}$. Applying (2.92), the expression for premixed flame velocity S_f could be written as

$$S_f = \mathrm{v}^* \cdot n - V_f = \frac{-u^* f_x + v^* - f_t}{\sqrt{1 + f_x^2}} \tag{2.96}$$

$$S_f = S_L \left(1 - \mathit{J} k\right) \tag{2.97}$$

in which S_L is the laminar premixed flame velocity, J is the Markstein length as well as $k = -\nabla \cdot n$ is the mean curvature. Laminar premixed flame velocity S_L, the propagation velocity of a premixed flame, is a exclusive property of a mixture, showing its reactivity and exothermicity in a provided diffusive medium. The Markstein length J is normally a coefficient of the order of the premixed flame thickness l_f and is depending on physico-chemical factors like the thermal expansion coefficient, Lewis number, equivalence ratio and global activation energy of the chemical reaction. The dependence of J on Lewis number is determined by the deficient reactant, i.e. it is dependent on Lewis number of the fuel in lean mixtures as well as Lewis number of the oxidant in rich mixtures.

Equations (2.91), (2.95) and (2.97) admit a simple solution in the form of a planar premixed flame located at $y = -S_L t$. The velocity and pressure across the premixed flame front are piecewise constants given by

$$v = \begin{cases} 0 & y < -S_L t \\ (\sigma - 1)\, S_L & y > -S_L t, \end{cases} \tag{2.98}$$

$$p = \begin{cases} 0 & y < -S_L t \\ -(\sigma - 1)\, \sigma_u {S_L}^2 & y > -S_L t, \end{cases} \tag{2.99}$$

in which $\sigma = \rho_u / \rho_b > 1$ will be the thermal expansion coefficient. An asymptotic solution which represents a weakly corrugated premixed flame can be received as a perturbation of the planar premixed flame for the limit of weak thermal expansion, i.e. $(\rho - 1) \ll 1$. The disturbed premixed flame front can be determined in the form

$$y = -S_L t + (\sigma - 1)\, \phi \tag{2.100}$$

in which $\phi = \phi(x, \tau)$ represents the premixed flame front and $\tau = (\sigma - 1)t$ is the scaled time. The speed is scaled as $\mathrm{v} = \overline{\mathrm{v}} + (1 - \sigma)^2 \widetilde{\mathrm{v}}$ and pressure as $\mathrm{p} = \overline{\mathrm{p}} + (1 - \sigma)^2 \widetilde{\mathrm{p}}$ where $\overline{\mathrm{v}}$, $\overline{\mathrm{p}}$ correspond to the basic state of the planar premixed flame. The premixed flame velocity relations (2.96) and (2.97) provide

$$\frac{-(\sigma - 1)^3 \phi_x \tilde{u} + (\sigma - 1)^2 \tilde{v}^* + S_L - (\sigma - 1)^2 \phi_\tau}{\sqrt{1 + (\sigma - 1)^2 {\phi_x}^2}} = S_L - \frac{S_L \mathit{J} (\sigma - 1)\, \phi_{xx}}{\sqrt{1 + (\sigma - 1)^2 {\phi_x}^2}}$$

where the curvature $\nabla \cdot n \approx -\phi_{xx}/\sqrt{1+(\sigma-1)^2{\phi_x}^2}$. Using the approximation

$$\sqrt{1+x^2} \simeq 1 + \frac{1}{2}x + \cdots$$

$$\sqrt{1+(\sigma-1)^2{\phi_x}^2} \simeq 1 + \frac{1}{2}(\sigma-1)^2{\phi_x}^2 + \cdots$$

and keeping terms of $O(\sigma-1)^2$ we get

$$S_L + (\sigma-1)^2\tilde{v}^* - (\sigma-1)^2\phi_\tau = S_L + \frac{1}{2}S_L(\sigma-1)^2{\phi_x}^2 - \mathcal{J}S_L(\sigma-1)\phi_{xx}$$

$$\phi_\tau + \frac{1}{2}S_L{\phi_x}^2 - \frac{S_L\mathcal{J}}{(\sigma-1)}\phi_{xx} - \tilde{v}^* = 0 \tag{2.101}$$

To evaluate v^* we will need to solve for the flow field. Prior to substituting the scaled expressions in the Euler equations, it is convenient to move to a coordinate system connected to the planar front. Let $\hat{y} = y - S_L t$ and then

$$\frac{\partial}{\partial t} = \frac{\partial}{\partial t} + S_L\frac{\partial}{\partial \hat{y}}, \quad \frac{\partial}{\partial \hat{y}} = \frac{\partial}{\partial y}.$$

The Euler equations can be written as

$$u_x + v_x = 0$$

$$\rho u_t + \rho u u_x + \rho(u+S_L)u_y = -p_x,$$

$$\rho v_t + \rho u v_x + \rho(v+S_L)u_y = -p_y.$$

Substituting the scaled expressions for pressure and speed in the Euler equations and keeping terms of $O(\sigma-1)^2$ we get

$$\tilde{u}_x + \tilde{v}_x = 0$$

$$\rho_u S_L\tilde{u}_y = -\tilde{p}_x,$$

$$\rho_u S_L\tilde{v}_y = -\tilde{p}_y.$$

These equations are valid for $\hat{y} > 0$ and $\hat{y} < 0$ since $\rho_b = \rho_u/\sigma = \rho_u/[1+(\sigma-1)] \sim \rho_u[1-(\sigma-1)] \sim \rho_u + O(\sigma-1)$.

The jump conditions throughout the disturbed premixed flame surface are listed by (2.95). Because the perturbation of the premixed flame surface is small, the jump

conditions are transferred throughout $y = 0$ by doing a Taylor expansion around $y = 0$. Keeping terms of $O(\sigma - 1)^2$ we obtain

$$\begin{aligned} [[\tilde{v}]] &= 0, \\ \left[\left[\tilde{u}\right]\right] &= -\phi_x, \\ [[\tilde{p}]] &= 0. \end{aligned} \tag{2.102}$$

Non-dimensionalizing the system with the transverse area of integration as the unit for length, S_L as the unit for speed, L/S_L as the unit for time and $\rho_u {S_L}^2$ as the unit for pressure we get

$$\tilde{u}_x + \tilde{v}_x = 0 \tag{2.103}$$

$$\tilde{u}_y = -\tilde{p}_x, \tag{2.104}$$

$$\tilde{v}_y = -\tilde{p}_y. \tag{2.105}$$

as the non-dimensionalized Euler equations. The non-dimensional evolution equation for the premixed flame profile can be described as

$$\phi_\tau + \frac{1}{2}{\phi_x}^2 - \alpha\phi_{xx} - \tilde{v}^* = 0 \tag{2.106}$$

The parameter $\alpha = \frac{\mathrm{J}}{L(\sigma-1)}$ is the scaled Markstein number and as observed from the expression, is inversely proportional to the transverse area of integration. Equations (2.104) and (2.105) jointly provide the following

$$\nabla^2 \hat{p} = 0. \tag{2.107}$$

The Fourier transform of a function, say $h(x, y, \tau)$, is provided by

$$\mathcal{F}\left(h\left(x, y, \tau\right)\right) \equiv h_k\left(y, \tau\right) = \int_{-\infty}^{\infty} e^{-ikx} h\left(x, y, \tau\right) dx, \tag{2.108}$$

and its inverse is provided by

$$h\left(x, y, \tau\right) = \frac{1}{2\pi} \int_{-\infty}^{\infty} e^{ikx} h_k\left(y, \tau\right) dk, \tag{2.109}$$

Using Fourier transform of (2.107) we get

$$\left(\tilde{p}_k\right)_{yy} - k^2 \tilde{p}_k = 0 \tag{2.110}$$

which solving on either of the surface results in

$$\tilde{p}_k = \begin{cases} C_1 e^{|k|y} & y < 0 \\ C_2 e^{-|k|y} & y > 0. \end{cases} \tag{2.111}$$

From (2.105),

$$(\tilde{v}_k)_y = \begin{cases} -|k|\, C_1 e^{|k|y} & y < 0 \\ |k|\, C_2 e^{-|k|y} & y > 0. \end{cases} \tag{2.112}$$

Integrating according to y,

$$\tilde{v}_k = \begin{cases} -C_1 e^{|k|y} + C_3 & y < 0 \\ -C_2 e^{-|k|y} + C_4 & y > 0. \end{cases} \tag{2.113}$$

Because the premixed flame is propagating in a quiescent flow, the speed field in the unburnt gases a long way away from the premixed flame front has a tendency to 0, i.e. $\lim_{y\to-\infty} \tilde{v} = 0$ which sets $C_3 = 0$, leading to

$$\tilde{v}_k = \begin{cases} -C_1 e^{|k|y} & y < 0 \\ -C_2 e^{-|k|y} + C_4 & y > 0. \end{cases} \tag{2.114}$$

From (2.103),

$$\tilde{u}_x = -\tilde{v}_y,$$

$$\tilde{u}_k = \frac{i}{k}\tilde{v}_k{}_y.$$

From (2.112),

$$\tilde{v}_k = \begin{cases} -\frac{|k|}{k} i C_1 e^{|k|y} & y < 0 \\ \frac{|k|}{k} C_2 e^{-|k|y} & y > 0. \end{cases} \tag{2.115}$$

Applying the jump conditions given by (2.102)–(2.111), (2.114) and (2.115) we get

$$C_1 = C_2 = -\frac{|k|}{2}\phi_k,$$

$$C_4 = 0.$$

Transforming into physical space via inverse Fourier transform, as shown in (2.109) we obtain

$$\tilde{v}^* = \frac{1}{4\pi}\int_{-\infty}^{\infty}\int_{-\infty}^{\infty}|k|\, e^{ik(x-\xi)}\phi\,(\xi,\tau)\,dkd\xi = \frac{1}{2}I\,\{\phi\} \tag{2.116}$$

The operator $I\,\{\phi\}$ is a linear operator that in Fourier constitutes a multiplication by $|k|$ i.e. $I\,\{\cos(kx)\} = |\mathrm{k}|\cos(kx)$. Equation (2.106) may at this point be written as

$$\phi_\tau + \frac{1}{2}{\phi_x}^2 - \alpha\phi_{xx} - \frac{1}{2}I\,\{\phi\} = 0 \tag{2.117}$$

This equation is well-known as the Michelson-Sivashinsky (MS) equation. Its dimensional form will be the following

$$\phi_\tau + \frac{1}{2}S_L{\phi_x}^2 - \frac{S_L\mathcal{J}}{(\sigma-1)}\phi_{xx} - \frac{1}{2}I\,\{\phi\} = 0 \tag{2.118}$$

http://www.springer.com/978-3-319-18844-7

Pole Solutions for Flame Front Propagation

Kupervasser, O.

2015, XII, 118 p. 37 illus., 10 illus. in color., Hardcover
ISBN: 978-3-319-18844-7